Kinetic Study of Thermal Decomposition of Sugarcane Bagasse Pseudo-Components at Typical Pretreatment Conditions: Towards the Establishment of a Feasible Primary Biorefining

Juliana Otavia Bahú
Universidade Estadual de Campinas - Campus Cidade Universitaria Zeferino Vaz: Universidade Estadual de Campinas

Leticia Mayuri Aiacyda De Souza
Federal University of Sao Paulo - Diadema Campus: Universidade Federal de Sao Paulo - Campus Diadema

Julio César de Jesus Gariboti
Universidade Federal de São Paulo - Campus Diadema Unidade José de Filippi: Universidade Federal de Sao Paulo - Campus Diadema

Elmer Ccopa Rivera
Andrews University

Romilda Fernandez Felisbino
Universidade Federal de São Paulo Instituto de Ciências Ambientais Químicas e Farmacêuticas: Universidade Federal de Sao Paulo - Campus Diadema

Rubens Maciel Filho
Universidade Estadual de Campinas - Campus Cidade Universitaria Zeferino Vaz: Universidade Estadual de Campinas

Laura Plazas Tovar (laura.tovar@unifesp.br)
Universidade Federal de São Paulo Instituto de Ciências Ambientais Químicas e Farmacêuticas: Universidade Federal de Sao Paulo - Campus Diadema https://orcid.org/0000-0003-1001-9250

Research Article

Keywords: sugarcane bagasse, biorefining, thermal degradation, TGA, model-free method, model fitting method

Posted Date: June 3rd, 2022

DOI: https://doi.org/10.21203/rs.3.rs-1692600/v1

Kinetic Study of Thermal Decomposition of Sugarcane Bagasse Pseudo-Components at Typical Pretreatment Conditions: Towards the Establishment of a Feasible Primary Biorefining

Juliana Otavia Bahú[1], Leticia Mayuri Aiacyda De Souza[2], Julio César de Jesus Gariboti[2], Elmer Ccopa Rivera[3], Romilda Fernandez Felisbino[2], Rubens Maciel Filho[1], Laura Plazas Tovar[1,2*]

[1] School of Chemical Engineering, University of Campinas, ZIP code 13083-852, Campinas-SP, Brazil.

[2] Department of Chemical Engineering, Federal University of São Paulo, ZIP code 09913-030, Diadema-SP, Brazil.

[3] Department of Engineering and Computer Science, Andrews University, Berrien Springs, MI, USA.

*To whom correspondence should be addressed: laura.tovar@unifesp.br

Abstract

A deeper understanding of the kinetics and thermodynamics parameters of sugarcane bagasse (SCB) thermal degradation could define appropriate conditions for primary biorefining in the production of renewable fuels. In this work, the kinetics of thermal degradation of SCB's high polymers are investigated through thermogravimetric data. From this data, model-free and model fitting methods are used to calculate apparent activation energies (E_a) and other related kinetic parameters. DTG curves present three major peaks associated with pseudo-components (PSEs): PSE 1 (hemicelluloses + extractives and lignin), PSE 2 (cellulose + extractives and lignin), and PSE 3 (lignin + extractives and residual holocelluloses). An essential advance is related to the quantitative interpretation of the degradation process by multi-stage modeling governed by diffusion-controlled reactions and order-based models. The Kissinger-Akahira-Sunose method provided E_a ranges of 124 – 154, 147 – 153, and 230 – 530 kJ·mol^{-1}, while the ranges obtained by the Flynn-Wall-Ozawa method were 120 – 152, 144 – 150, and 232 – 545 kJ·mol^{-1}, both for PSE 1, PSE 2, and PSE 3, respectively. Data could support the calculation of many critical operating parameters in biorefinery process, such as the pretreatment minimum temperature. SCB biorefining could lead to a degradation of up to 10, 0.5, and 11 % for PSE 1, PSE 2, and PSE 3, respectively, at 473.15 K for 200 min. Thermodynamic parameters (ΔH, ΔG, and ΔS) determined SCB endothermic and non-spontaneous thermal degradation.

Keywords: sugarcane bagasse, biorefining, thermal degradation, TGA, model-free method, model fitting method.

1. Introduction

A difficult task to produce lignocellulosic-based biofuels relies on the compositional and structural barriers of the lignocellulosic materials, which urges solutions in the biomass refining strategies used to enhance the fermentable sugars' yielding [1]. Selective separation of the major lignocellulosic constituents (cellulose, hemicelluloses, and lignin) is mandatory to rupture the cellulose-hemicelluloses-lignin complex through primary biorefining (pretreatment and biomass conditioning) [2]. Such treatments minimize the lignocellulosic biomass recalcitrance, however, it is necessary to evaluate the impact of the operating conditions of these primary biorefining methods on the carbohydrate outcome from biomass pretreatment for further processing and valuation.

Some changes might occur in the intrinsic compositional and physical/chemical structure of the cellulose, hemicelluloses, and lignin after the pretreatments. Including, increase in the accessible surface area, reduction in the crystallinity degree of cellulose, removal of hemicelluloses and lignin polymers [3]. However, most of the published literature shows insufficient information on the effects of the pretreatment operating conditions on the loss of its major constituents due to thermal degradation. Interestingly, some research groups observed that the concentration of monomers detected does not match the solubilized polysaccharides concentration after pretreatment of sugarcane bagasse [4, 5]. These results revealed a lower yield of fermentable sugar according to certain operating conditions (temperature, residence time, and acid concentration) during the biomass pretreatment [6].

Several functions for the most common mechanisms in solid-state reactions such as random nucleation and growth of nuclei, phase boundary controlled reaction, dimensional diffusion, and reaction-order models have been proposed [7, 8]. For decades, researchers overlooked these models regarding studying thermal degradation, mainly adopting the reaction-order models to describe this process [9, 10]. However, some analyses forced kinetic data into empirical reaction-order model obtaining an unappropriated representation of the degradation process. The significant variation of apparent activation energies and pre-exponential factors clearly show that thermal degradation involves multiple reactions that should be handled through a model of multiple reactions in parallel.

A complicating factor in this regard is that considerable losses of the major biomass constituents occur due to thermal degradation during the primary biorefining [11, 12]. A deeper understanding of the kinetics and thermodynamics related to that type of degradation could support the calculation of the critical operating parameters, such as the pretreatment minimum temperature [13]. In addition, this knowledge would lead to a prospective study to overcome the structural and compositional barriers of lignocellulosic material during biorefining [14]. The experimental and simulation studies could focus on the following aspects:

- Study of the effects of different pretreatments on the compositional characteristics of the pseudo-components (PSEs), which can be designated as PSE 1 (hemicelluloses + extractives and lignin), PSE 2 (cellulose + extractives and lignin), and PSE 3 (lignin + extractives and residual holocellulose);
- Reduction of PSEs loss due to thermal degradation, which leads to a decrease in yields of fermentable sugars (from cellulose and hemicelluloses);

- Avoid discrepancies in material balances.

The centerpiece in the kinetic modeling of the thermal degradation is critical to predict the sugarcane bagasse's behavior under various operating parameters during the primary biorefining. It also collaborates for the understanding of the thermal degradation process and clarifies the loss of its major constituents (here referred to as PSEs) [15]. The acceptance of non-isothermal methods is highly motivated because just one non-isothermal experiment can provide the same information as an isothermal method, which usually employs a set of experiments at different temperatures [16]. Besides, the isoconversional models have been used successfully for the estimation of kinetic parameters of several materials [17, 18]. Then, an adequate systematic kinetic analysis of the solid-state mechanism must be resultant of an evaluation of the thermal degradation kinetics under various temperature programming (**Table 1**), enabling detail of the kinetic parameters of this process and also evaluating the results' reliability [19].

This study investigated the kinetics of thermal degradation of the major constituents from sugarcane bagasse (SCB) by three parallel one-step multi reactions in apparent kinetic models. Three model-free non-isothermal methods (Kissinger, Kissinger-Akahira-Sunose (KAS), and Flynn-Wall-Ozawa (FWO) methods) were used to estimate the apparent activation energy ($E_{a,i}$) and Arrhenius pre-exponential factor (A_i) as a function of conversion degree (α). Although the most significant contribution of this work is the estimation of kinetic parameters of the degradation process, there is no doubt that the degradation process does not strictly hold a single-step approximation and also that it might reveal a significant variation in their kinetic parameters. Several solid-state kinetic models (**Table 1**) are analyzed and compared to describe the degradation mechanism and transform that mathematically into a rate equation. The thermodynamic analysis also confirmed the complexity of the SCB thermal degradation mechanism. Finally, carbohydrate and lignin losses due to the thermal degradation process are assessed under certain operating conditions (temperature and residence time) looking for a sustainable primary biorefining. Moreover, these data can be used to develop computational models for the conversion of biomass, which is important to encourage the development of new biorefinery technologies.

2. Materials and Methods

2.1. Materials and Sample Preparation

Sugarcane bagasse (SCB) with a moisture content of 52.2 wt % was kindly provided by the São João sugar mill, Araras, São Paulo, Brazil. The moisture content was reduced to 5.0 – 5.5 wt % after five days of natural drying under atmospheric conditions. The SCB was then grounded using an A-11 basic analytical mill equipped with a cutting blade (for pulverizing soft, fibrous grinding materials, IKA® Werke Staufen/Germany), and sieved to a maximum particle size of 0.21 mm. The grounded samples were dried in a drying oven with air renewal circulation (SP LABOR, Brazil) at 378.15 K (± 1.0) for 24 h prior to further analyses. The composition in terms of structural carbohydrates and lignin (41.8 ± 3.3 % cellulose; 31.0 ± 2.5 % hemicelluloses; 17.1 ± 3.4 % lignin; 2.5 ± 0.1 % ash; 9.0 ± 0.1 % extractives) was determined according to the standard National Renewable Energy Laboratory (NREL) protocols based on a two-step acid hydrolysis [20]. The samples were kept in a desiccator at room temperature before the thermogravimetric analysis.

2.2. Thermogravimetric Analysis

The thermogravimetric analysis was carried out under dynamic conditions using a Shimadzu TGA-50 Series (Shimadzu Corporation, International Marketing Division, Tokyo-Japan), equipped with a microbalance and a high-temperature furnace (measurement temperature range: ambient to 1273.5 K). The analyzer was operated from a computer equipped with TA-50 WSI thermal analysis workstation. The mass and temperature calibrations of the TGA-50 Series analyzer were performed according to the manufacturer's recommendations. The milled samples were conditioned in platinum crucibles, each sample weighing 16.00 ± 0.5 mg. The furnace was purged with an inert atmosphere (N_2 flow rate = 50 mL·min^{-1}) at room temperature and atmospheric pressure. The experiments were carried out from room temperature to 378.15 K using a heating rate of 10 K·min^{-1}, remaining at the final temperature (378.15 K) for 10 min. This was implemented to ensure that the run began with a dry sample. The isothermal hold at 378.15 K also guaranteed that all samples started with the same temperature distribution and thermal equilibrium. Subsequently, the samples were heated from 378.15 K to 1173.15 K at four programmed heating rates: 10, 20, 30, and 40 K·min^{-1}.

2.3. Signal Processing (Deconvolution)

The derivative thermogravimetric (DTG) curves were deconvoluted into three different peaks (PSE 1, PSE 2, and PSE 3) using iterative fits of the Gaussian distribution function. This procedure allowed obtaining information about the reaction mechanisms and a complete kinetic description through the estimation of the kinetic parameters. Peak deconvolution was performed using the Levenberg-Marquardt algorithm in Microcal Origin® 8.0 software (MicroCal Inc., Northampton, MA, USA), and deviations up to ± 8 % were obtained when compared to the experimental data.

2.4. Kinetic, Theoretical Aspects, and Thermodynamics Parameters Calculation

The kinetic parameters of the thermal degradation of SCB (based on that of the PSE) were calculated from the TG and DTG curves. Since SCB contains heterogeneous materials (biomass-derived polymers), we believe that the degradation process involves numerous reactions occurring separately, due to the biomass composition complexity. It is thus impossible to know the details of individual reactions.

Generally, the thermal degradation can be expressed by the overall reaction described in **Figure 1**. A parallel independent reaction model could describe the decomposition of SCB. The degradation of the individual SCB pseudo-components can be expressed by:

$$\frac{d\alpha}{dt} = A_i e^{\left(\frac{E_{a,i}}{RT}\right)} f(\alpha) \qquad \text{Equation 1}$$

Where α is the degree of conversion, t is the reaction time, A_i and $E_{a,i}$ are the pre-exponential factor, and the activation energy of each reaction in **Figure 1**, respectively, R is the universal gas constant, T is the absolute temperature, and $f(\alpha)$ is the reaction model.

The degree of conversion (α) represents the decomposed amount of biomass and it can be defined as:

$$\alpha = \frac{m_0 - m_t}{m_0 - m_f} \quad \text{Equation 2}$$

Where m_0 is the sample initial mass, m_t is the sample mass at time t, and m_f is the sample final mass.

Considering a constant heating rate (β, commonly used in TG experiments) where T changes linearly with t: $\beta = dT/dt$, Equation 1 is rearranged as follow:

$$\frac{d\alpha}{\mathrm{dT}} = \frac{A_i}{\beta} e^{\left(\frac{E_{a,i}}{RT}\right)} f(\alpha) \quad \text{Equation 3}$$

Integrating Equation 3 with respect to the temperature yields:

$$g(\alpha) = \int_0^{\alpha} \frac{d\alpha}{f(\alpha)} = \frac{A_i}{\beta} \int_0^{T} e^{\left(\frac{E_{a,i}}{RT}\right)} dT \quad \text{Equation 4}$$

Different solid-state kinetic models in their integral and differential forms are presented in **Table 1** [21, 22].

2.4.1. Parameter Estimation Procedure: Model Free-Method

The model-free method assumes that the thermal degradation reaction rate is only a function of temperature (T). The parameters $E_{a,i}$ and A_i that characterize each reaction, in **Figure 1**, are constant for a specific β and α. Hence, the model free-method allows one to estimate the kinetic parameters $E_{a,i}$ and A_i at a specific α, for an independent kinetic function. Repeating this procedure throughout the conversion degree range, it is possible to obtain a profile of the activation energy as a function of α. Otherwise, the Kissinger method considers the condition of maximum conversion rate to estimate the parameters.

Kissinger Method

The kinetic parameters determined by the Kissinger method are based on the study of the rate equation at the maximum reaction rate, which means that $\frac{d^2\,\alpha}{d\,t^2}$ is equal to zero Equation 5 [23].

$$\frac{d^2\,\alpha}{d\,t^2} = \left(\frac{E_{a,i}\beta}{RT_m^2} + A_i f'(\alpha_m)\, exp\left(\frac{-E_{a,i}}{RT_m}\right)\right)\left(\frac{d\,\alpha}{d\,t}_m\right) = 0 \quad \text{Equation 5}$$

Where T_m is the temperature at the maximum peak on the DTG curve, α_m is the conversion degree, and T_m, $\frac{d\,\alpha}{d\,t}_m$ is the maximum reaction.

The Kissinger method is also based on the following equation:

$$ln\left(\frac{\beta}{T_m^2}\right) = ln\left(\frac{-A_i R}{E_{a,i}} f'(\alpha_m)\right) - \frac{E_{a,i}}{R}\frac{1}{T_m} \quad \text{Equation 6}$$

Where the $E_{a,i}$ is determined from the DTG data at different heating rates by linear regression of the $ln\left(\frac{\beta}{{T_m}^2}\right)$ versus T_m^{-1} plot. The A_i is estimated using the expressions $f(\alpha)$ and their first derivatives ($f'(\alpha)$), for the kinetic models used to describe the solid-state reactions in **Table 1**.

Kissinger-Akahira-Sunose (KAS) Method

The KAS method for determining the $E_{a,i}$ dependence on α ($E_{a,i\alpha}$) is presented in Equation 7 [24].

$$ln\left(\frac{\beta_j}{T_{\alpha,j}^2}\right) \cong \left(ln\frac{RA_{i,\alpha}}{E_{a,i_\alpha}} - ln\, g\,(\alpha)\right) - \frac{E_{a,i_\alpha}}{RT_{\alpha,j}} \quad \text{Equation 7}$$

The plot of $ln\left(\frac{\beta_j}{T_{\alpha,j}^2}\right)$ versus $\frac{1}{T_{\alpha,j}}$, obtained from experiments recorded at several heating rates (β_i), should be a straight line with a slope of $-\frac{E_{a,i_\alpha}}{R}$.

Flynn-Wall-Ozawa (FWO) Method

Using Doyle's approximation $ln\, p\,(\alpha) \cong -5.3305 - 1.0516\alpha$ in the α interval from 0.2 - 0.6, an approximate integral method for determining the dependence of $E_{a,i}$ on α ($E_{a,i\alpha}$) was based on the method developed by FWO [25].

$$ln\,\beta_j \cong -1.0516\frac{E_{a,i_\alpha}}{RT_{\alpha,j}} + \left(ln\frac{E_{a,i_\alpha}A_{\alpha,i}}{R} - ln\, g\,(\alpha) - 5.3305\right) \quad \text{Equation 8}$$

Thus, from the plot of the left side of Equation 8 versus $\frac{1}{T_{\alpha,j}}$, obtained from the curves recorded during multiple constant heating rates (β_j) at constant conversion, the slope can be used to evaluate the activation energy (approximately $-1.0516\frac{E_{a,i_\alpha}}{RT_{\alpha,j}}$).

In both cases, that is the KAS and FWO methods, *g(α)* is the integral form of the kinetic models used to describe the solid-state mechanism shown in **Table 1**; $A_{\alpha,i}$ is the pre-exponential factor at constant α; E_{a,i_α} is the activation energy at constant α.

2.4.2. Thermodynamic Parameters

Data and information from using the Kissinger, FWO, and KAS model-free methods allowed the estimation of the thermodynamic parameters of SCB thermal degradation (based on PSE), including the changes of enthalpy (ΔH), free Gibbs energy (ΔG), and entropy (ΔS) [26].

The thermodynamic parameters (ΔH, ΔG, and ΔS), in Equation 9 – 11, were estimated at each β using the Kissinger method. Otherwise, they were estimated at 10 K·min^{-1} to reduce the effect of the interaction during the thermal degradation [27].

$$\Delta H = E_{a,i} - RT_\alpha \quad \text{Equation 9}$$

$$\Delta G = E_{a,i} + RT_m\, ln\left(\frac{K_B T_m}{hA_i}\right) \quad \text{Equation 10}$$

$$\Delta S = \frac{\Delta H - \Delta G}{T_m} \quad \text{Equation 11}$$

Where, K_B represents the Boltzmann constant (1.381×10^{-23} J·K^{-1}), h is the Plank constant (6.626×10^{-34} J·s), and T_α is the temperature at specific α.

2.4.3. A Kinetic Model for Thermal Degradation of the Major Constituents from SCB

The kinetic model corresponding to three parallel one-step multi reactions in **Figure 1** can be described by the following system of ordinary differential equations:

$$\frac{d\,\alpha_1}{d\,t} = A_{\alpha,1}\, e^{\left(\frac{-E_{a,1}}{RT}\right)} f\,(\alpha_1) \qquad \text{Equation 12}$$

$$\frac{d\,\alpha_2}{d\,t} = A_{\alpha,2}\, e^{\left(\frac{-E_{a,2}}{RT}\right)} f\,(\alpha_2) \qquad \text{Equation 13}$$

$$\frac{d\,\alpha_3}{d\,t} = A_{\alpha,3}\, e^{\left(\frac{-E_{a,3}}{RT}\right)} f\,(\alpha_3) \qquad \text{Equation 14}$$

Where $f(\alpha_i)$ is the form of the function describing the reaction model (**Table 1**). The $E_{a,i}$ and $A_{\alpha,i}$ are kinetic parameters estimated from the model-free FWO method as a function of α.

The overall degradation rate can be obtained by summing up the rate equations of individual reactions as Equation 15:

$$\frac{d\,\alpha}{d\,t} = \sum_{i=1}^{3} \lambda_i A_i\, exp\left(\frac{-E_{a,i}}{RT}\right) f(\alpha) \qquad \text{Equation 15}$$

Where λ_i is the mass loss contribution of constituent i, which is defined as the relative fraction of the area under the i^{th} DTG PSE peak.

The overall DTG curve fitting can be achieved by adding DTG PSE peaks by minimizing the objective function (OF) through the non-linear least square method defined as Equation 16 [28]:

$$OF = \sum \left(\frac{d\,\alpha}{d\,t}\bigg|_{exp} - \frac{d\,\alpha}{d\,t}\bigg|_{cal} \right)^2 \qquad \text{Equation 16}$$

Where $\frac{d\,\alpha}{d\,t}\big|_{exp}$ and $\frac{d\,\alpha}{d\,t}\big|_{cal}$ are experimental and calculated values by the proposed model conversion rates, respectively.

The quality of the model-fit can be determined in terms of *fit (%)* as Equation 17

$$fit(\%) = \left[1 - \frac{\sqrt{\overline{OF}}}{\left(\frac{d\,\alpha}{d\,t}\big|_{exp}\right)_m} \right] \times 100 \qquad \text{Equation 17}$$

Where $\overline{OF}$ is the average of the OF, and $\left(\frac{d\,\alpha}{d\,t}\big|_{exp}\right)_m$ is the peak maximum value of the degradation rate.

The iterative calculation process used to solve ordinary differential equations was carried out by a discretization procedure for the time (as the independent variable) with a minimum value of 101 points, which gives a trade-off between higher–accuracy discretization. The resulting system was solved using the fifth/fourth-order Runge Kutta Fehlberg (RKF45) numerical method. The iterative computation process was implemented using the FORTRAN 90 language, and the FORTRAN code was compiled and executed by a Compaq® FORTRAN compiler to get the outputs of the degraded fraction from the major constituents from SCB.

3. Results and discussion

3.1. Thermogravimetric Analysis and Deconvolution Peaks

The differential mass loss (DTG) curves recorded for SCB at four heating rates (10, 20, 30, and 40 K·min^{-1}) under an atmosphere (N_2) are presented in **Figure 2**. As expected, the SCB mass diminished with heating as a result of thermal degradation. Four zones were identified, where several reactions took place. The DTG results show an initial zone where the light volatiles were liberated, and the water evaporation process occurred at temperatures below 450 K. Following, there was thermal degradation of the major constituents from biomass, which proceeded from approximately 450 to 711 K (at 10 K·min^{-1}, **Figure 2a**), 450 to 722 K (at 20·K·min^{-1}, **Figure 2b**), 450 to 733 K (at 30 K·min^{-1}, **Figure 2c**), and 450 to 744 K (at 40·K·min^{-1}, **Figure 2d**). Two overlapping peaks, related to two PSEs, could be identified in the main degradation zone. Moreover, above 711 K for the lower heating rate, and above 744 K for the higher heating rate, another zone known as the minor degradation zone, related to PSE 3, could be visualized.

The degradation process proceeded faster from 450 to 700 K (second step) with steep slopes of the TG curves were noted. The last remarkable steepness explains the significant loss in mass, due to both faster degradation of the PSE 1 and PSE 2, and the liberation of volatile hydrocarbons. The loss in mass then decreased up to 1173.15 K. The experimental results reported that the solid residue yields were about 17.50 % for SCB.

In an effort to better identify the zones related to the thermal degradation of the biomass constituents (associated with the PSEs) and their overlapping kinetics at four heating rates, the thermogravimetric data were processed by "deconvolution" of the overlapping peaks by means of the Levenberg–Marquardt´s non-linear optimization method using the gauss multi-peak equation. The comparison of the experimental DTG curves with the results after the deconvolution procedure is shown in **Figure 2**. The adjusted R squared (adjusted-R^2) values were above 0.99 for each heating rate (data not shown in this work). SCB is comprised mainly of hemicelluloses, cellulose, and lignin as the major constituents. These biomass polymers were identified at different stages of mass loss as depicted in **Figure 3**. The peaks show the mass loss rate represented by the DTG curves, recorded during the degradation process of the PSEs at different heating rates. The degradation process described in **Figure 1** consisted of three parallel one-step multi reactions (Rxn) as follows:

- Rxn1: Associated with hemicelluloses + extractives and lignin. The degradation process occurs at a temperature range from 500 to 700 K with a maximum rate between 605 and 636 K, depending on the heating rate (**Figure 3a**). Researchers have reported that hemicelluloses typically decompose in the range of 433 to 613 K [29, 30].
- Rxn2: Associated with cellulose + extractives and lignin. The degradation process occurs at a temperature range from 650 to 750 K with a maximum rate between 656 and 690 K depending on the heating rate (**Figure 3b**). Furthermore, it is important to highlight that PSE 2 mainly degrades at a higher temperature and narrower temperature zone than PSE 1, suggesting that the degradation rate of PSE 2 is more sensitive to temperature than PSE 1 [31, 32].
- Rxn3: Associated with lignin + extractives and residual holocellulose (hemicelluloses + cellulose). The degradation process occurs at a slower rate (when compared to the mass losses

of PSE 1 and PSE 2) over a much wider temperature range, from 400 to 1050 K, with a maximum rate between 683 and 691 K depending on the heating rate (**Figure 3c**) [31].

Thus, the sequence of thermal degradation was: PSE 1 (at 450 – 700 K) > PSE 2 (at 650 – 700) > PSE 3 (at 450 – 1050 K). Nevertheless, the degradation of PSE 3 occurred from 450 up to 1050 K, due to its more thermally stable nature as compared to PSE1 and PSE 2. On the other hand, PSE 2 degraded at higher temperatures but in a narrower temperature zone than PSE 1, suggesting that the degradation rate of PSE 2 was more sensitive to temperature than PSE 1. Finally, the total mass loss at the final temperature of 1050 K was 82.50 %.

Besides considering individually these PSEs from biomass, they have a biological function in the plant cells, as their organization consists of celluloses microfibers involved with hemicelluloses, altogether surrounded by lignin, forming a complex tridimensional structure that enhances the plant mechanical strength [33]. An explanation of the PSEs' thermal behavior relies on their constituents (PSEs) [34]. Hemicelluloses have branched pentoses in their polymeric chain, implying a lower thermal temperature degradation [35]. While cellulose is major constituted of hexoses, in a linear arrangement, resulting in greater thermal stability in comparison to hemicelluloses, however as a result of homogeneous chain structure and high crystallinity, it has a narrower thermal profile [36]. On the other hand, lignin that intensifies the recalcitrance of the biomass, is a heterogeneous, phenolic polymer, with highly aromatic chains, that presents the most thermal stability among the PSEs [37, 38]. Another assumption that can be made for these PSEs is that due to the crystalline structure of cellulose, this PSE 1 directly affects the kinetic parameters ($E_{a,i}$) since more heat is required to thermal activate this highly organized component. Furthermore, the amorphous structure of lignin confers the final tail at the TG curve profile, lowering its PSE 3 - $E_{a,i}$ to a wide temperature range, to form the lignin char [39].

The kinetic analysis of the thermal degradation was carried out by model-free methods as described earlier, based on the fact that an understanding of the degradation process from the biomass PSEs is required to determine the loss of major constituents from the SCB under the operational conditions of time and temperature.

3.2. Estimation of Kinetic Parameters and Mechanism Analysis

The properties of three peaks obtained at four heating rates (10, 20, 30, and 40 K·min^{-1}) were summarized in **Table 2**. The results demonstrated that all the peaks or deflections shifted proportionally towards higher reaction temperatures with the heating rates, which means that the peak temperature (T_m), peak height (H_m), and conversion at T_m (α_m) were dependent on the heating rate. Thus, the variations in the properties of the three peaks with the heating rate account for the three parallel one-step multi reactions of PSE 1, PSE 2, and PSE 3, respectively (**Figure 1**).

The model-free method proposed by Kissinger to calculate the $E_{a,i}$, and A_i, from the DTG data at four heating rates (10, 20, 30, and 40·K min^{-1}) was used in this work. The kinetic data were obtained from the peaks of the DTG curves (**Figure 3**), assuming different kinetic functions ($f(\alpha)$) to estimate A_i. According to this assumption, the plot $ln\left(\frac{\beta}{T_m^2}\right)$ versus ${T_m}^{-1}$ should be a straight line, where the slope allows one to calculate the E_{ai}. This plot was constructed for each PSE and the results are shown in **Figure 4**.

The data obtained for the kinetic parameters ($E_{a,i}$, and A_i) were statistically analyzed to find the degree of reliability, and the results can be seen in **Table 2**. The values obtained for the $E_{a,i}$ and A_i of the three PSEs were derived from the slope and intercept, respectively, and were all of linear fit. Regarding the estimation of the $E_{a,i}$, it is clear that this is a positive value and does not depend on the heating rate. The $E_{a,i}$ values were within the ranges reported for each PSE in **Table 2**. For the PSE 1, PSE 2, and PSE 3, the values obtained by the Kissinger method for the $E_{a,i}$ were about 135; 139; and 328 kJ·mol^{-1}, respectively. Hence the sequence for the $E_{a,i}$ of the biomass PSEs is: PSE 3 > PSE 2 > PSE 1. The A_i estimated for the thermal degradation of the SCB's PSEs varied over a wide range, since six kinetic functions, $f(\alpha)$, were used (R2, R3, F1, D2, D3, and A2, in **Table 1**) as shown in **Table 2**.

To confirm the values obtained using the Kissinger method and avoid erroneous values in the set of parameters obtained for the $E_{a,i}$ and A_i using the different kinetic functions, $f(\alpha)$, the kinetic results were compared with the data obtained using the FWO and KAS methods.

Thus, the model-free method established a dependence of the $E_{a,i}$ on the conversion rate, α [40].

The quantitative kinetic analysis carried out using iso-conversional methods is based on conversion–temperature data, thus the conversion degree (α) plot against the temperature produces sigmoid curves **Figure 3**.

In the α versus temperature curves, three different profiles (sigmoid curves) were identified, associated with the kinetics of thermal degradation of the three PSEs. Consequently, three regions confirmed the zones shown in the DT/DTG curves, characterized as lower conversion rates, being no bigger than 2.0, 4.0, and 8.0 % for PSE 1, PSE 2, and PSE 3, respectively. In the next section of the α versus temperature curves, the conversion rate in the ranges 500 – 700 K (for PSE 1), 650 – 750 K (for PSE 2), and 500 – 900 K (for PSE 3), was more intense in the evaluated range, as regards the volatilization of complex organic molecules and/or hydrocarbons. The third stage of these curves appeared at 700 K for PSE 1 and PSE 2, and at 900 K for PSE 3, since the conversion with temperature is at its lowest value, probably the degradation process is almost finished.

In order to study the thermal effect on the three parallel thermal degradation reactions of the three PSEs at four heating rates (10, 20, 30, and 40 K·min^{-1}), the KAS and FWO model-free methods were used to estimate the kinetic parameters (E_{a,i_α} and $A_{\alpha,i}$) as a function of the conversion degree, α.

In this study, ten conversion degree values of 0.05 – 0.9 (equivalent to 5 – 90 %) with an increment of 0.1 (or 10 %) after 0.1, under each heating rate condition were analyzed. **Figure 5** shows the estimates for the kinetic parameters, for the whole set of α values used in the linear plot, as determined using the FWO and KAS methods. **Table 3** gives an overview of the adjusted-R^2 values corresponding to the linear fit data in **Figure 5**, together with the values obtained for the E_{a,i_α} and $A_{\alpha,i}$, at each conversion degree (between $0.05 < \alpha < 0.9$) in the thermal degradation of PSE 1, PSE 2, and PSE 3.

In both cases, it is important to remember that the FWO and KAS methods apply an integral approximation, valid between $0.2 < \alpha < 0.6$ and $0.2 < \alpha < 0.5$, respectively. Thus, the kinetic parameters estimated out of the valid ranges may not show a physical and/or mathematical sense (being a specific case of kinetic data obtained for the thermal degradation of PSE 3 at a conversion degree greater than 0.6).

From the data obtained for the adjusted-R^2 shown in **Table 3**, it can be seen that both the FWO and KAS methods performed well during the fit of the linear regression data, and the E_{a,i_α} values estimated

from these two methods are close to each other at the same α. This confirms that the methods studied in this work can be used to calculate the kinetic parameters. This was also demonstrated in studies of the thermal stages of SCB [33], petroleum derived [41], polymers [42], and other biomass types [43].

Analyzing Rxn1, related to the thermal degradation of PSE 1, it can be seen that the linear profiles (for the FWO and KAS plots) were nearly parallel in the conversion range of $0.2 < \alpha < 0.8$, which implies the chance of a single degradation reaction mechanism or a multi-reaction mechanism. However, in the ranges below or equal to 0.2 and above or equal to 0.8, the degradation reactions may be different, due to the lack of parallelism of the lines. In consequence, the iso-conversion analyses indicated variations in both E_{a,i_α} and $A_{\alpha,i}$ values, with an increase in the conversion degree, α. This observation provides evidence that the degradation process of PSE 1 takes place in multi-steps. In contrast, the degradation process of PSE 2 corresponds to a single step reaction or a multi-reaction mechanism, since there was little variation in the E_{a,i_α} values (147 – 153 kJ·mol^{-1} by the KAS method, and 144 – 150 kJ·mol^{-1} by the FWO method) with an increase in the conversion degree.

On the other hand, the thermal degradation rate of PSE 3 was identified as a complex reaction, showing changes in the apparent activation energy with increases in the conversion degree. This change will depend on: (i) the contribution of each compound present in PSE 3 (lignin + extractives and residual holocellulose), (ii) the complexity of the degradation reaction(s), and (iii) the multi-step reactions.

3.3. Estimation of Thermodynamic Parameters

Thermodynamic parameters are significant to adequately design reactors on a larger scale for primary biorefining processes. According to the results of the last section, the $E_{a,i}$ derived from model-free methods (**Table 2** and **Table 3**) were used to calculate the thermodynamic parameters (ΔH, ΔG, and ΔS) (**Table 2**and **Table 3**).

The enthalpy (ΔH) changes revealed the energy difference between the reagent and the activated complex [26]. Moreover, a positive ΔH indicates that energy is required for the reactants to reach their transition state, implying that the thermal degradation reactions were all endothermic [26]. As seen in **Table 2** and **Table 3**, the value of ΔH increases with α. The average values of ΔH for PSE 1, PSE 2, and PSE 3 are 141.7, 144.7, and 300.8 kJ·mol^{-1}, respectively, for FWO method; 139.1, 141.3, and 306.4 kJ·mol^{-1}, respectively, for KAS method. The results demonstrated that more heat energies are required for PSE 3 degradation process than PSE 1 and PSE 2 to dissociate the reagents bonds, which agrees with $E_{a,i}$ derived from the model-free method.

The changes of the Gibbs free energy (ΔG) reflect the energy variation of the reactional system to approximate the molecules and form the activated complex [44], which means that the process is endergonic and not spontaneous in the forward direction. During the thermal degradation, by ΔG it is possible to evaluate the disorder change, where low ΔG values favors the reaction. Furthermore, ΔG has no noticeable change for PSE 1 and PSE 2. The average values of ΔG for PSE 1, PSE 2, and PSE 3 are 323.5, 343.1, and 454.5 kJ·mol^{-1}, respectively, for FWO method; 321.1, 339.9, and 457.4 kJ·mol^{-1}, respectively, for KAS method. With these, the favorability order of the degradation process was PSE 1 > PSE 2 > PSE 3. Then, PSE 1 and PSE 2 consumed a great portion of heating in the degradation process, disordering the system, and favoring the degradation process.

The entropies (ΔS) had negative variation values (**Table 2** and **Table 3**), indicating a lower degree of disorder of the products compared to the initial PSEs in the thermal degradation process (**Figure 1**).

All in all, as thermal degradation is endothermic, $\Delta H > 0$, and the entropy of the system decreases, $\Delta S < 0$, the sign of ΔG is positive at all temperatures. Thus, the degradation process is never spontaneous.

3.4. Thermal Degradation Model with Focus on Primary Biorefining Processes

Based on FWO and KAS method, it is possible to highlight that when $\alpha > 0.05$, it is an indicator that the thermal degradation begins to occur in PSE 1 and the amorphous portion of the PSE 2 structure, allowing an increase in the E_a values. Hence, PSE 1 had a specific reaction heating, where during its degradation, high levels of CO_2 are formed, whereas in lower contents are formed CO, methanol, methane, furfural, 5-hydroxymethylfurfural, and anhydrous sugars produced in substantial amounts from other polysaccharides [45, 46]. The degradation of cellulose, here referred to as PSE 2, is decomposed into levoglucosan, hydroxyacetaldehyde, hydroxylactone, pyruvic aldehyde, glyceraldehyde, 5-hydroxymethyl-furfural, and furfural, involving activation energy lower than 211·kJ·mol^{-1} [12, 46]. This indicates that PSE 1 and PSE 2 have lower thermal stability, though, PSE 3 has the highest thermal stability, degrading in a wider temperature range.

As seen in **Table 1**, the solid-state kinetic models are identified into four groups: A_n, R_n, D_n, and F_n, respectively, these mechanisms describe: random nucleation, nuclei growth, phase boundary controlled reaction, dimensional diffusion, and reaction-order models. Using the average E_a obtained from the model-free method, the mass loss contribution (λ_i), in Equation 15, was estimated and mentioned in **Table 4**. The difference between the experimental and predicted values ($\frac{d\alpha}{dt}\Big|_{exp}$ and $\frac{d\alpha}{dt}\Big|_{cal}$) are reported as indicated by OF and Fit (%). The simulated $\frac{d\alpha}{dt}\Big|_{cal}$ curves as a function of temperature from different solid-state kinetic models are illustrated in **Figure 6** and the corresponding optimized parameters are included in **Table 4**.

Comparing $\frac{d\alpha}{dt}\Big|_{exp}$ and $\frac{d\alpha}{dt}\Big|_{cal}$, the experimental data overlapped the D2, D3, and F1 heterogeneous kinetic models. According to literature, these heterogeneous mechanisms refer to a diffusion process in two and three dimensions, D2 and D3 respectively. They are related to the heat transfer capacity along with the material structure and order-based models representing simple models as they are similar to those used in homogeneous kinetics [47]. Similar results were described by for other biomasses [48]. In addition, thermal degradation follows a reaction-order model (F1) which is the simplest model as it is similar to those used in homogeneous kinetics. However, a misconception may be the result of approximating the degradation of PSEs from SCB towards A2, R2, or R3 heterogeneous kinetic models.

In order to advance and confirm the thermal degradation of major constituents associated with PSE 1, PSE 2, and PSE3, respectively, during the primary biorefining of SCB, different operating conditions were evaluated (**Figure 7**). Changes in biomass could be observed in the evolution of the profiles of the PSEs and the percent of degradation is used as an indicator of the liberation of thermally degraded fractions (TDF). The values for TDF were between 0.0 - 35 % (**Figure 7a**), 0.0 - 0.6 % (**Figure 7b**) and 0.9 - 16 % (**Figure 7c**) for PSE 1, PSE 2, and PSE 3, respectively, when considering a temperature range from 393.15 - 503.15 K, and 240 min.

It can be seen in **Figure 7** that each PSE exhibited a very different thermal degradation behavior. PSE 1 (**Figure 7a**), and PSE 3 (**Figure 7c**) tended to produce relatively high levels of TDF up to 100 min. On the other hand, PSE 1 produced significantly less TDF than PSE 3. Nevertheless, at temperatures above 483.15 K, the degradation process exhibited relatively high levels of TDF when compared to PSE 1. PSE 2 tended to produce relatively low levels of TDF (**Figure 7b**).

It is important to mention that higher temperatures than 503 K were not analyzed since this would represent roasting [49], and pyrolysis [40] of the biomass. Thus, a great deal of reaction mechanism information is required to properly model these processes. More accurate and detailed models can be assumed as presented in the published literature [50].

Thermal degradation was shown to have a great influence on the major biomass constituents as hemicelluloses (PSE 1), cellulose (PSE 2), and lignin (PSE 3). One of the motivations of this work was to explore how the temperature and time, during primary biorefining, affected the degradation of the biomass constituents. The results showed that the effect of temperature and time on the degradation process was important and should be considered when primary biorefining SCB (i. e. acid-catalyzed hydrothermal pretreatment, hydrothermal pretreatment, organosolv, and ammonia fiber expansion (AFEX)), as they can directly affect the availability of fermentable sugars.

In the conception of SCB, a byproduct generated by the agricultural sugar-alcohol industry in the production of biofuels, and an economical alternative for the sustainable production of electricity (co-generation), it is important to minimize TDF, since the thermal degradation of biomass fuels is related to their major constituents (i.e., considering the degradation behavior of cellulose, hemicelluloses, and lignin under the combination of time and temperature in the operating conditions). We believe that TDF below 5 % in the primary biorefining process is acceptable in the processing of SCB. In the field of research into primary biorefining, this approach could be useful, since the degradation of the major constituents from biomass is still unknown. This thermal degradation model will be incorporated into the global physicochemical conversion of SCB and material balances.

Conclusions

The DTG curves showed that thermal degradation of sugarcane bagasse (SCB) did not occur in a single reaction. This behavior was evidenced by the three parallel one-step multi reaction overlapping peaks corresponding to three pseudocomponents (PSEs): PSE 1 (hemicelluloses + extractives and lignin), PSE 2 (cellulose + extractives and lignin), and PSE 3 (lignin + extractives and residual holocellulose). The ranges of the apparent activation energies were specified for each model-free method. The Kissinger method reported approximately 135, 139, and 328 $kJ \cdot mol^{-1}$, respectively, for PSE 1, PSE 2, and PSE 3; but offered no information about the multi-step or complex reactions taking place during the thermal degradation process. It was, therefore, useful to apply the Flynn-Wall-Ozawa (FWO) and Kissinger-Akahira-Sunose (KAS) model-free methods. The KAS method reported the variability of the apparent activation energy values as 124 – 154, 146 – 153, and 230 – 530 $kJ \cdot mol^{-1}$; and the FWO method reported values of 120 – 152, 144 – 150, and 232 – 545 $kJ \cdot mol^{-1}$, respectively, for PSE 1, PSE 2, and PSE 3. Thus, the degradation of PSE 3 occurred from as low as 450 K and up to 1050 K, due to its more thermally stable nature as compared

to PSE1 and PSE 2. On the other hand, the degradation of PSE 2 was more sensitive to temperature than that of PSE 1. The thermodynamic parameters (positive ΔH, positive ΔG, and negative ΔS) were determined by the activated complex theory. These validated that the degradation process of SCB major constituents was endothermic and non-spontaneous. Consequently, thermal degradation of the major constituents of SCB is governed by diffusion models (i.e., two and three-dimensional diffusion - Jander equation) and reaction-order models (i.e., first-order or unimolecular decay law). The thermally degraded fractions (TDF) in the establishment of sustainable primary biorefining can attain up to 5%. Combining knowledge of the TDF and the material balances it will be possible to minimize the mismatches in the amount of solubilized polysaccharides in front of detected sugar concentrations and recovery of the high polymers (cellulose, hemicelluloses, and lignin) from biomass.

Acknowledgements

The authors are grateful for the support by FAPESP (São Paulo Research Foundation) [grant numbers 2015/20630-4 and 2012/10857-3] and National Council for Scientific and Technological Development [grant n° 408149/2018-3].

References

1. Struhs E, Mirkouei A, Ramirez-Corredores MM, et al (2021) Overview and Technology Opportunities for Thermochemically-Produced Bio-Blendstocks. J Environ Chem Eng 9:106255. https://doi.org/10.1016/j.jece.2021.106255
2. Guragain YN, Vadlani P V (2021) Renewable Biomass Utilization: A Way Forward to Establish Sustainable Chemical and Processing Industries. Clean Technol 3:243–259. https://doi.org/10.3390/cleantechnol3010014
3. Sidana A, Yadav SK (2022) Recent Developments in Lignocellulosic Biomass Pretreatment with a Focus on Eco-Friendly, Non-Conventional Methods. J Clean Prod 335:130286. https://doi.org/10.1016/j.jclepro.2021.130286
4. Rocha GJM, Martín C, da Silva VFN, et al (2012) Mass Balance of Pilot-Scale Pretreatment of Sugarcane Bagasse by Steam Explosion Followed by Alkaline Delignification. Bioresour Technol 111:447–452. https://doi.org/10.1016/j.biortech.2012.02.005
5. Sabiha-Hanim S, Halim NAA (2019) Sugarcane Bagasse Pretreatment Methods for Ethanol Production. In: Basso TP, Basso LC (eds) Fuel Ethanol Production from Sugarcane. IntechOpen, Rijeka
6. Chambon CL, Mkhize TY, Reddy P, et al (2018) Pretreatment of South African Sugarcane Bagasse using a Low-Cost Protic Ionic Liquid: A Comparison of Whole, Depithed, Fibrous and Pith Bagasse Fractions. Biotechnol Biofuels 11:1–16. https://doi.org/10.1186/s13068-018-1247-0
7. Khawam A, Flanagan DR (2006) Basics and Applications of Solid-State Kinetics: A Pharmaceutical Perspective. J Pharm Sci 95:472–498. https://doi.org/10.1002/jps.20559
8. Kodani S, Koga N (2020) Kinetics of Contracting Geometry-Type Reactions in the Solid State: Implications from the Thermally Induced Transformation Processes of α-Oxalic Acid Dihydrate. Phys Chem Chem Phys 22:19560–19572. https://doi.org/10.1039/D0CP03176C
9. Mothé CG, De Miranda IC (2013) Study of Kinetic Parameters of Thermal Decomposition of Bagasse and Sugarcane Straw Using Friedman and Ozawa-Flynn-Wall Isoconversional Methods. J Therm Anal Calorim 113:497–505. https://doi.org/10.1007/s10973-013-3163-7

10. Orfão JJM, Antunes FJA, Figueiredo JL (1999) 99/03241 Pyrolysis Kinetics of Lignocellosic Materials—Three Independent Reactions Model. Fuel Energy Abstr 40:340. https://doi.org/10.1016/s0140-6701(99)91196-7

11. Goldšteins L, Valdmanis R, Zaķe M, et al (2021) Thermal Decomposition and Combustion of Microwave Pre-Treated Biomass Pellets. Processes 9:. https://doi.org/10.3390/pr9030492

12. Shen D, Zhang L, Xue J, et al (2015) Thermal Degradation of Xylan-Based Hemicellulose under Oxidative Atmosphere. Carbohydr Polym 127:363–371. https://doi.org/10.1016/j.carbpol.2015.03.067

13. Ruiz HA, Galbe M, Garrote G, et al (2021) Severity Factor Kinetic Model as a Strategic Parameter of Hydrothermal Processing (Steam Explosion and Liquid Hot Water) for Biomass Fractionation under Biorefinery Concept. Bioresour Technol 342:125961. https://doi.org/10.1016/j.biortech.2021.125961

14. de Paula Protásio T, da Costa JS, Scatolino M V, et al (2021) Revealing the Influence of Chemical Compounds on the Pyrolysis of Lignocellulosic Wastes from the Amazonian Production Chains. Int J Environ Sci Technol. https://doi.org/10.1007/s13762-021-03416-w

15. Emiola-Sadiq T, Zhang L, Dalai AK (2021) Thermal and Kinetic Studies on Biomass Degradation via Thermogravimetric Analysis: A Combination of Model-Fitting and Model-Free Approach. ACS Omega 6:22233–22247. https://doi.org/10.1021/acsomega.1c02937

16. Vyazovkin S (2018) Modern Isoconversional Kinetics: From Misconceptions to Advances, 2nd ed. Elsevier B.V.

17. Mishra RK, Mohanty K (2018) Pyrolysis Characteristics and Kinetic Parameters Assessment of Three Waste Biomass. J Renew Sustain Energy 10:. https://doi.org/10.1063/1.5000879

18. Luo L, Guo X, Zhang Z, et al (2020) Insight into Pyrolysis Kinetics of Lignocellulosic Biomass: Isoconversional Kinetic Analysis by the Modified Friedman Method. Energy & Fuels 34:4874–4881. https://doi.org/10.1021/acs.energyfuels.0c00275

19. Millán LMR, Vargas FES, Nzihou A (2017) Kinetic Analysis of Tropical Lignocellulosic Agrowaste Pyrolysis. Bioenergy Res 10:832–845. https://doi.org/10.1007/s12155-017-9844-5

20. Sluiter A, Hames B, Ruiz R, et al (2008) Determination of Structural Carbohydrates and Lignin in Biomass - NREL/TP-510-42618. Natl Renew Energy Lab 17

21. Ishida T, Gokon N, Hatamachi T, Kodama T (2014) Kinetics of Thermal Reduction Step of Thermochemical Two-Step Water Splitting Using CeO2 Particles: Master-Plot Method for Analyzing Non-Isothermal Experiments. Energy Procedia 49:1970–1979. https://doi.org/10.1016/j.egypro.2014.03.209

22. Vyazovkin S, Chrissafis K, Di Lorenzo ML, et al (2014) ICTAC Kinetics Committee Recommendations for Collecting Experimental Thermal Analysis Data for Kinetic Computations. Thermochim Acta 590:1–23. https://doi.org/10.1016/j.tca.2014.05.036

23. Fedunik-Hofman L, Bayon A, Donne SW (2019) Kinetics of Solid-Gas Reactions and Their Application to Carbonate Looping Systems. Energies 12:. https://doi.org/10.3390/en12152981

24. Morais LC, Maia AAD, Guandique MEG, Rosa AH (2017) Pyrolysis and Combustion of Sugarcane Bagasse. J Therm Anal Calorim 129:1813–1822. https://doi.org/10.1007/s10973-017-6329-x

25. Ma Z, Chen D, Gu J, et al (2015) Determination of Pyrolysis Characteristics and Kinetics of Palm Kernel Shell Using TGA-FTIR and Model-Free Integral Methods. Energy Convers Manag 89:251–259. https://doi.org/10.1016/j.enconman.2014.09.074

26. Huang L, Liu J, He Y, et al (2016) Thermodynamics and Kinetics Parameters of Co-Combustion between Sewage Sludge and Water Hyacinth in CO2/O2 Atmosphere as Biomass to Solid Biofuel. Bioresour Technol 218:631–642. https://doi.org/10.1016/j.biortech.2016.06.133

27. Yuan X, He T, Cao H, Yuan Q (2017) Cattle Manure Pyrolysis Process: Kinetic and Thermodynamic Analysis with Isoconversional Methods. Renew Energy 107:489–496. https://doi.org/10.1016/j.renene.2017.02.026

28. Ali I, Naqvi SR, Bahadar A (2018) Kinetic Analysis of Botryococcus braunii Pyrolysis Using Model-Free and Model Fitting Methods. Fuel 214:369–380.

https://doi.org/10.1016/j.fuel.2017.11.046

29. Aboyade AO, Hugo TJ, Carrier M, et al (2011) Non-Isothermal Kinetic Analysis of the Devolatilization of Corn Cobs and Sugar Cane Bagasse in an Inert Atmosphere. Thermochim Acta 517:81–89. https://doi.org/10.1016/j.tca.2011.01.035

30. Aboyade AO, Carrier M, Meyer EL, et al (2012) Model Fitting Kinetic Analysis and Characterisation of the Devolatilization of Coal Blends with Corn and Sugarcane Residues. Thermochim Acta 530:95–106. https://doi.org/10.1016/j.tca.2011.12.007

31. Jumaidin R, Zainel SNM, Adam NW, et al (2021) Thermal Degradation and Mecahnical Characteristics of Sugarcane Bagasse Reinforced Biodegradable Potato Starch Composites. J Adv Res Fluid Mech Therm Sci 78:157–166. https://doi.org/10.37934/arfmts.78.1.157166

32. Machado G, Santos F, Faria D, et al (2018) Characterization and Potential Evaluation of Residues from the Sugarcane Industry of Rio Grande do Sul in Biorefinery Processes. Nat Resour 9:175–187. https://doi.org/10.4236/nr.2018.95011

33. Wang J, Yellezuome D, Zhang Z, et al (2022) Understanding Pyrolysis Mechanisms of Pinewood Sawdust and Sugarcane Bagasse from Kinetics and Thermodynamics. Ind Crops Prod 177:114378. https://doi.org/10.1016/j.indcrop.2021.114378

34. Taşar Ş (2021) Thermal Conversion Behavior of Cellulose and Hemicellulose Fractions Isolated from Tea Leaf Brewing Waste: Kinetic and Thermodynamic Evaluation. Biomass Convers Biorefinery. https://doi.org/10.1007/s13399-021-01697-2

35. Dulie NW, Woldeyes B, Demsash HD, Jabasingh AS (2021) An Insight into the Valorization of Hemicellulose Fraction of Biomass into Furfural: Catalytic Conversion and Product Separation. Waste and Biomass Valorization 12:531–552. https://doi.org/10.1007/s12649-020-00946-1

36. Acharya S, Liyanage S, Parajuli P, et al (2021) Utilization of Cellulose to Its Full Potential: A Review on Cellulose Dissolution, Regeneration, and Applications. Polymers (Basel) 13:. https://doi.org/10.3390/polym13244344

37. López-Beceiro J, Díaz-Díaz AM, Álvarez-García A, et al (2021) The Complexity of Lignin Thermal Degradation in the Isothermal Context. Processes 9:. https://doi.org/10.3390/pr9071154

38. Ornaghi HL, Ornaghi FG, Neves RM, et al (2020) Mechanisms Involved in Thermal Degradation of Lignocellulosic Fibers: A Survey based on Chemical Composition. Cellulose 27:4949–4961. https://doi.org/10.1007/s10570-020-03132-7

39. Ballice L, Sert M, Sağlam M, Yüksel M (2020) Determination of Pyrolysis Kinetics of Cellulose and Lignin Fractions Isolated from Selected Turkish Biomasses. Arab J Sci Eng 45:7429–7444. https://doi.org/10.1007/s13369-020-04594-4

40. Abdelouahed L, Leveneur S, Vernieres-Hassimi L, et al (2017) Comparative Investigation for the Determination of Kinetic Parameters for Biomass Pyrolysis by Thermogravimetric Analysis. J Therm Anal Calorim 129:1201–1213. https://doi.org/10.1007/s10973-017-6212-9

41. Wang Z, Gong Z, Wang Z, et al (2022) Gasification Characteristics and Kinetic Analysis of Oily Sludge. J Therm Anal Calorim. https://doi.org/10.1007/s10973-022-11278-8

42. Handawy MK, Snegirev AY, Stepanov V V, Talalov VA (2021) Kinetic Modeling and Analysis of Pyrolysis of Polymethyl Methacrylate using Isoconversional Methods. {IOP} Conf Ser Mater Sci Eng 1100:12053. https://doi.org/10.1088/1757-899x/1100/1/012053

43. Bhattacharjee N, Biswas AB (2020) Physicochemical Analysis and Kinetic Study of Orange Bagasse at Higher Heating Rates. Fuel 271:117642. https://doi.org/10.1016/j.fuel.2020.117642

44. Chen J, Wang Y, Lang X, et al (2017) Evaluation of Agricultural Residues Pyrolysis Under Non-Isothermal Conditions: Thermal Behaviors, Kinetics, and Thermodynamics. Bioresour Technol 241:340–348. https://doi.org/10.1016/j.biortech.2017.05.036

45. Werner K, Pommer L, Broström M (2014) Thermal Decomposition of Hemicelluloses. J Anal Appl Pyrolysis 110:130–137. https://doi.org/10.1016/j.jaap.2014.08.013

46. Yogalakshmi KN, Poornima Devi T, Sivashanmugam P, et al (2022) Lignocellulosic Biomass-Based Pyrolysis: A Comprehensive Review. Chemosphere 286:131824. https://doi.org/10.1016/j.chemosphere.2021.131824

47. Khawam A, Flanagan DR (2006) Solid-State Kinetic Models: Basics and Mathematical Fundamentals. J Phys Chem B 110:17315–17328. https://doi.org/10.1021/jp062746a

48. Burnham AK, Zhou X, Broadbelt LJ (2015) Critical Review of the Global Chemical Kinetics of Cellulose Thermal Decomposition. Energy and Fuels 29:2906–2918. https://doi.org/10.1021/acs.energyfuels.5b00350

49. Bates RB, Ghoniem AF (2013) Biomass Torrefaction: Modeling of Reaction Thermochemistry. Bioresour Technol 134:331–340. https://doi.org/10.1016/j.biortech.2013.01.158

50. Blondeau J, Jeanmart H (2012) Biomass Pyrolysis at High Temperatures: Prediction of Gaseous Species Yields from an Anisotropic Particle. Biomass and Bioenergy 41:107–121. https://doi.org/10.1016/j.biombioe.2012.02.016

Declaration of Interest

The authors declare that are no financial competing interests.

Authors Contribution

Bahú, J.O.: Conceptualization, Visualization, Writing - Original Draft, Review & Editing; Gariboti, J.C.J., Rivera, E.C., Lopes, E.S., Lopes, M.S., Felisbino, R.F.: Writing - Original Draft; Maciel Filho, R.: Supervision, Project Administration; Tovar, L.P.: Data Collection, Analysis, Conceptualization, Supervision, Writing - Original Draft, Review & Editing. All authors read and approved the final manuscript.

Data Availability

The datasets generated during and/or analyzed during the current study are available from the corresponding author, prof. dr. Laura Plazas Tovar, laura.tovar@unifesp.br, on reasonable request.

625 **Table 1** Models (*f(α)*) used in the heterogeneous kinetics, their first derivatives (*f'(α)*), and the integral form ($g(\alpha)=\int_0^{\alpha}\frac{\mathrm{d}\alpha}{f(\alpha)}$) examined in this work

Reaction model	**Code**	**f(α)**	**f'(α)**	**g(α)**
Random nucleation and nuclei growth				
Avarami-Erofe'ev	A2	$2\times(1-\alpha)\times[-\ln(1-\alpha)]^{1-1/2}$	$[2\times\ln(1-\alpha)+2-1]/\{[-\ln(1-\alpha)]^{1/2}\}$	$[-\ln(1-\alpha)]^{1/2}$
Phase boundary-controlled reaction				
Contracting area (*i.e.*, bidimensional shape)	R2	$(1-\alpha)^{1/2}$	$-1/[2\times(1-\alpha)^{1/2}]$	$[1-(1-\alpha)^{1/2}]$
Contracting volume (*i.e.*, tridimensional shape)	R3	$(1-\alpha)^{2/3}$	$-2/[3\times(1-\alpha)^{1/3}]$	$[1-(1-\alpha)^{1/3}]$
Diffusion models				
Two-dimensional diffusion	D2	$[-\ln(1-\alpha)]^{-1}$	$-1/\{[\ln(1-\alpha)]^2\times(1-\alpha)\}$	$[(1-\alpha)\times\ln(1-\alpha)]+\alpha$
Three-dimensional diffusion (Jander equation)	D3	$[3\times(1-\alpha)^{2/3}]/\{2\times[1-(1-\alpha)^{1/3}]\}$	$[0.5-(1-\alpha)^{-1/3}]/[1-(1-\alpha)^{1/3}]^2$	$[1-(1-\alpha)^{1/3}]^2$
Reaction-order models				
First-order (unimolecular decay law)	F1	$(1-\alpha)$	-1	$-\ln(1-\alpha)$

626

Table 2 The properties of three peaks of the SCB sample' PSEs obtained at four heating rates (10, 20 30, and 40 K·min^{-1}), and values estimated (apparent activation energy, E_a, and pre-exponential factor, A) using the Kissinger method for the adjusted-R^2

Parameters type			**PSE1**				**PSE 2**				**PSE 3**			
Heating rate, β (K·min^{-1})			10	20	30	40	10	20	30	40	10	20	30	40
Peak temperature, T_m (K)			605.8	620.3	631.0	635.7	656.3	672.6	684.2	690.6	683.1	683.9	689.3	691.6
Peak height, H_m (K^{-1})			0.014	0.026	0.038	0.055	0.023	0.039	0.054	0.074	0.001	0.002	0.004	0.006
Conversion at T_m, α_m (-)			0.488	0.501	0.509	0.514	0.496	0.514	0.523	0.533	0.476	0.487	0.49	0.491
Kinetic	E_{ai} (kJ·mol^{-1})		134.6				138.9				328.1			
	ln A_i (min^{-1}) using different $f(\alpha)$ kinetic functions	R2	26.3	26.2	26.2	26.2	24.9	24.8	24.8	24.8	58.6	58.6	58.6	58.6
		R3	26.1	26.1	26.1	26.1	24.7	24.7	24.7	24.7	58.4	58.4	58.4	58.4
		F1	25.9				24.5				58.2			
		D2	24.4	24.5	24.5	24.5	23.1	23.1	23.2	23.2	56.7	56.7	56.8	56.8
		D3	23.0	23.0	23.1	23.1	21.6	21.7	21.7	21.8	55.2	55.3	55.3	55.3
		A2	26.8	26.7	26.6	26.6	25.3	25.2	25.1	25.0	59.2	59.1	59.1	59.1
	Adjusted-R^2		0.993				0.998				0.963			
Thermodynamic	ΔH (kJ·mol^{-1})		129.5	129.4	129.3	129.3	133.4	133.3	133.2	133.1	322.4	322.4	322.4	322.4
	ΔG (kJ·mol^{-1}) using different $f(\alpha)$ models	R2	311.3	315.7	318.9	320.3	331.1	336.0	339.5	341.4	523.5	523.7	525.3	526.0
		R3	311.3	315.7	318.9	320.3	331.1	336.0	339.5	341.5	523.5	523.8	525.4	526.1
		F1	311.4				331.2				523.5			
		D2	311.7	316.0	319.2	320.6	331.5	336.4	339.9	341.8	523.7	523.9	525.5	526.2
		D3	312.0	316.3	319.5	320.9	331.9	336.8	340.3	342.2	523.8	524.1	525.7	526.4
		A2	311.2	315.6	318.8	320.2	331.0	335.9	339.4	341.4	523.4	523.7	525.3	526.0
	ΔS (kJ·mol^{-1}·K^{-1}) using different $f(\alpha)$ models	R2	-300.1	-300.3	-300.4	-300.5	-301.2	-301.4	-301.5	-301.6	-294.4	-294.4	-294.5	-294.5
		R3	-300.1	-300.3	-300.5	-300.5	-301.2	-301.4	-301.6	-301.7	-294.4	-294.4	-294.5	-294.5
		F1	-300.2				-301.3				-294.4			
		D2	-300.7	-300.8	-301.0	-301.0	-301.8	-302.0	-302.1	-302.2	-294.7	-294.7	-294.7	-294.8
		D3	-301.2	-301.3	-301.5	-301.5	-302.3	-302.5	-302.6	-302.7	-294.9	-294.9	-294.9	-295.0
		A2	-299.9	-300.1	-300.3	-300.4	-301.0	-301.3	-301.5	-301.5	-294.3	-294.3	-294.4	-294.4

A_i in min^{-1}

Table 3 Values for the adjusted-R^2, apparent activation energy (E_{a,i_α}), pre-exponential factor ($A_{\alpha,i}$), and thermodynamic parameters, including the changes of enthalpy (ΔH), free Gibbs energy (ΔG), and entropy (ΔS) estimated using the FWO and KAS methods

Method	PSE	α	Kinetic parameters								Thermodynamic parameters												
			E_{ai} (kJ·mol^{-1})	Adj.-R^2	ln A_i (min^{-1})						ΔH (kJ·mol^{-1})	ΔG (kJ·mol^{-1})						ΔS (J·mol^{-1}·K^{-1})					
					R2	R3	F1	D2	D3	A2		R2	R3	F1	D2	D3	A2	R2	R3	F1	D2	D3	A2
FWO	PSE 1	0.05	104.5	0.993	18.4	18.0	19.1	15.4	13.9	20.5	99.9	283.0	283.1	282.8	283.9	284.4	282.5	-302.3	-302.5	-302.0	-303.8	-304.6	-301.4
		0.1	113.5	0.994	20.5	20.1	21.2	18.2	16.7	22.3	108.8	291.5	291.6	291.3	292.1	292.5	291.1	-301.6	-301.7	-301.3	-302.6	-303.3	-300.9
		0.2	123.9	0.994	22.8	22.4	23.5	21.2	19.7	24.3	119.0	301.3	301.4	301.2	301.7	302.0	301.0	-300.9	-301.0	-300.6	-301.5	-302.1	-300.4
		0.3	132.1	0.994	24.4	24.1	25.2	23.3	21.9	25.7	127.2	309.2	309.3	309.1	309.5	309.8	309.0	-300.4	-300.6	-300.2	-300.8	-301.3	-300.0
		0.4	139.0	0.994	25.8	25.4	26.6	24.9	23.6	26.9	134.0	315.8	315.9	315.7	316.0	316.3	315.6	-300.1	-300.2	-299.8	-300.4	-300.8	-299.7
		0.5	146.6	0.994	27.2	26.9	28.1	26.6	25.3	28.3	141.6	323.2	323.3	323.0	323.3	323.6	323.0	-299.7	-299.9	-299.5	-299.9	-300.4	-299.4
		0.6	154.4	0.993	28.6	28.3	29.5	28.2	26.9	29.6	149.3	330.7	330.8	330.6	330.8	331.0	330.6	-299.4	-299.5	-299.2	-299.6	-299.9	-299.2
		0.7	163.7	0.993	30.2	29.9	31.2	29.9	28.8	31.1	158.5	339.7	339.8	339.5	339.8	340.0	339.6	-299.1	-299.2	-298.8	-299.2	-299.5	-298.9
		0.8	177.7	0.992	32.6	32.3	33.6	32.4	31.4	33.4	172.4	353.4	353.4	353.2	353.4	353.5	353.2	-298.6	-298.7	-298.4	-298.7	-298.9	-298.4
		0.9	211.9	0.986	38.4	38.1	39.6	38.3	37.5	39.2	206.5	386.8	386.8	386.6	386.8	386.9	386.7	-297.5	-297.6	-297.2	-297.5	-297.7	-297.3
	PSE 2	0.05	152.4	0.986	24.7	24.3	25.4	21.7	20.2	26.9	147.2	344.6	344.7	344.5	345.3	345.7	344.2	-300.9	-301.0	-300.7	-302.0	-302.5	-300.2
		0.1	154.8	0.994	25.5	25.1	26.2	23.2	21.7	27.3	149.5	346.8	346.9	346.7	347.3	347.7	346.4	-300.7	-300.8	-300.5	-301.5	-302.0	-300.1
		0.2	153.3	0.996	25.6	25.3	26.4	24.1	22.6	27.1	148.0	345.4	345.4	345.2	345.7	346.0	345.1	-300.8	-300.9	-300.5	-301.3	-301.8	-300.3
		0.3	151.8	0.997	25.6	25.2	26.4	24.4	23.0	26.9	146.4	343.8	343.9	343.6	344.0	344.4	343.5	-300.8	-301.0	-300.6	-301.2	-301.7	-300.4
		0.4	149.7	0.998	25.4	25.0	26.2	24.5	23.1	26.5	144.3	341.8	341.9	341.6	342.0	342.3	341.5	-300.9	-301.1	-300.7	-301.2	-301.7	-300.6
		0.5	148.6	0.998	25.3	24.9	26.1	24.6	23.3	26.3	143.2	340.7	340.8	340.6	340.9	341.2	340.5	-301.0	-301.1	-300.7	-301.2	-301.7	-300.7
		0.6	147.3	0.998	25.1	24.8	26.0	24.7	23.4	26.1	141.9	339.5	339.5	339.3	339.6	339.8	339.3	-301.1	-301.2	-300.8	-301.3	-301.7	-300.8
		0.7	146.5	0.998	25.0	24.7	26.0	24.7	23.6	25.9	141.0	338.7	338.8	338.5	338.8	339.0	338.5	-301.2	-301.3	-300.9	-301.3	-301.7	-300.9
		0.8	146.0	0.998	24.9	24.6	26.0	24.8	23.7	25.7	140.4	338.2	338.2	337.9	338.2	338.4	338.0	-301.3	-301.4	-300.9	-301.3	-301.7	-301.0
		0.9	150.5	0.994	25.6	25.4	26.8	25.6	24.7	26.4	144.9	350.6	350.6	350.3	350.6	350.8	350.4	-301.2	-301.3	-300.8	-301.2	-301.5	-300.9
	PSE 3	0.05	149.6	0.993	33.1	32.7	33.8	30.1	28.6	35.3	145.6	348.2	348.3	348.1	348.8	349.1	347.9	-296.7	-296.8	-296.5	-297.5	-297.9	-296.2
		0.1	176.0	0.994	36.7	36.3	37.4	34.4	32.9	38.5	171.6	374.1	374.1	374.0	374.4	374.7	373.8	-296.4	-296.5	-296.3	-297.0	-297.3	-296.0
		0.2	230.3	0.994	45.1	44.7	45.9	43.5	42.1	46.6	225.4	427.2	427.2	427.1	427.4	427.6	427.0	-295.4	-295.5	-295.3	-295.7	-296.0	-295.1
		0.3	284.8	0.994	53.5	53.1	54.2	52.3	50.9	54.8	279.6	480.8	480.8	480.7	480.9	481.0	480.6	-294.4	-294.5	-294.3	-294.6	-294.9	-294.2
		0.4	347.5	0.994	62.9	62.6	63.7	62.0	60.7	64.1	342.0	542.5	542.5	542.4	542.6	542.7	542.4	-293.5	-293.5	-293.4	-293.6	-293.8	-293.3
		0.5	423.3	0.994	74.1	73.7	75.0	73.5	72.2	75.1	417.6	617.4	617.4	617.3	617.4	617.5	617.3	-292.5	-292.5	-292.4	-292.6	-292.7	-292.4
		0.6	529.9	0.993	89.7	89.4	90.6	89.2	88.0	90.7	523.9	722.9	722.9	722.8	722.9	723.0	722.8	-291.3	-291.3	-291.2	-291.3	-291.4	-291.2
KAS	PSE 1	0.05	100.4	0.992	17.2	16.8	17.9	14.2	12.7	19.4	95.8	279.3	279.4	279.1	280.3	280.8	278.7	-302.9	-303.1	-302.5	-304.5	-305.4	-301.9
		0.1	109.7	0.993	19.4	19.0	20.1	17.1	15.6	21.3	105.0	288.0	288.1	287.8	288.6	289.1	287.5	-302.0	-302.2	-301.7	-303.1	-303.8	-301.3
		0.2	120.4	0.994	21.8	21.4	22.6	20.2	18.8	23.3	115.6	298.1	298.2	297.9	298.4	298.8	297.7	-301.2	-301.4	-300.9	-301.9	-302.5	-300.7
		0.3	128.9	0.993	23.6	23.3	24.4	22.5	21.1	24.9	124.0	306.2	306.3	306.0	306.5	306.8	305.9	-300.7	-300.8	-300.4	-301.1	-301.7	-300.3
		0.4	136.1	0.993	25.1	24.7	25.9	24.2	22.8	26.2	131.1	313.0	313.1	312.9	313.2	313.5	312.8	-300.3	-300.5	-300.1	-300.6	-301.1	-300.0
		0.5	143.9	0.993	26.6	26.2	27.4	25.9	24.6	27.6	138.9	320.6	320.7	320.5	320.7	321.0	320.4	-300.0	-300.1	-299.7	-300.2	-300.6	-299.6
		0.6	152.0	0.992	28.0	27.7	29.0	27.6	26.4	29.0	146.9	328.4	328.5	328.3	328.5	328.7	328.3	-299.6	-299.7	-299.3	-299.7	-300.1	-299.3
		0.7	161.6	0.992	29.7	29.4	30.7	29.4	28.3	30.6	156.4	337.7	337.8	337.6	337.8	338.0	337.6	-299.2	-299.3	-299.0	-299.3	-299.6	-299.0
		0.8	176.2	0.991	32.2	32.0	33.3	32.1	31.1	33.1	171.0	351.9	352.0	351.8	351.9	352.1	351.8	-298.7	-298.8	-298.4	-298.7	-299.0	-298.5
		0.9	212.0	0.985	38.3	38.1	39.5	38.3	37.5	39.1	206.6	386.8	386.8	386.6	386.8	386.9	386.7	-297.5	-297.6	-297.2	-297.5	-297.7	-297.3
	PSE 2	0.05	149.6	0.984	24.0	23.6	24.7	21.1	19.6	26.2	144.4	342.0	342.1	341.8	342.7	343.1	341.5	-301.1	-301.2	-300.9	-302.2	-302.8	-300.4
		0.1	152.0	0.993	24.9	24.5	25.6	22.6	21.1	26.7	146.7	344.1	344.2	344.0	344.7	345.0	343.8	-300.9	-301.1	-300.7	-301.7	-302.3	-300.3
		0.2	150.4	0.996	25.0	24.6	25.7	23.4	21.9	26.5	145.0	342.5	342.6	342.4	342.9	343.2	342.2	-301.0	-301.1	-300.7	-301.5	-302.1	-300.5
		0.3	148.6	0.997	24.9	24.5	25.6	23.7	22.3	26.1	143.2	340.8	340.9	340.6	341.0	341.4	340.5	-301.1	-301.2	-300.8	-301.5	-302.0	-300.6
		0.4	146.4	0.997	24.6	24.2	25.4	23.7	22.4	25.7	140.9	338.6	338.7	338.4	338.8	339.1	338.4	-301.2	-301.3	-300.9	-301.5	-302.0	-300.8
		0.5	145.2	0.998	24.5	24.1	25.3	23.8	22.6	25.5	139.7	337.5	337.5	337.3	337.6	337.9	337.2	-301.3	-301.4	-301.0	-301.5	-302.0	-300.9
		0.6	143.8	0.998	24.3	24.0	25.2	23.8	22.6	25.2	138.3	336.1	336.1	335.9	336.2	336.5	335.9	-301.4	-301.5	-301.1	-301.5	-302.0	-301.1
		0.7	142.8	0.998	24.2	23.8	25.1	23.9	22.7	25.0	137.3	335.2	335.3	335.0	335.3	335.5	335.0	-301.5	-301.6	-301.2	-301.6	-302.0	-301.2
		0.8	142.2	0.997	24.0	23.8	25.1	23.9	22.9	24.9	136.6	334.6	334.6	334.3	334.6	334.8	334.4	-301.6	-301.7	-301.2	-301.6	-302.0	-301.3
		0.9	146.8	0.993	24.8	24.5	26.0	24.7	23.9	25.6	141.1	347.1	347.1	346.8	347.1	347.3	346.9	-301.5	-301.5	-301.1	-301.5	-301.7	-301.2
	PSE 3	0.05	149.1	0.992	32.9	32.5	33.6	29.9	28.4	35.1	145.0	347.7	347.8	347.6	348.3	348.6	347.4	-296.8	-296.9	-296.6	-297.6	-298.0	-296.2
		0.1	176.1	0.993	36.7	36.3	37.4	34.4	32.9	38.5	171.7	374.2	374.3	374.1	374.6	374.8	373.9	-296.4	-296.5	-296.3	-297.0	-297.3	-296.0
		0.2	232.4	0.993	45.5	45.1	46.2	43.9	42.5	47.0	227.5	429.2	429.3	429.1	429.4	429.6	429.0	-295.3	-295.4	-295.2	-295.6	-295.9	-295.1
		0.3	289.2	0.990	54.1	53.8	54.9	53.0	51.6	55.4	283.9	485.0	485.0	484.9	485.1	485.3	484.9	-294.3	-294.4	-294.2	-294.5	-294.7	-294.1
		0.4	354.6	0.986	63.9	63.5	64.7	63.0	61.7	65.1	349.1	549.5	549.5	549.4	549.6	549.7	549.4	-293.4	-293.4	-293.2	-293.5	-293.6	-293.2
		0.5	433.8	0.979	75.4	75.0	76.3	74.7	73.5	76.4	428.1	627.8	627.8	627.7	627.8	627.9	627.7	-292.4	-292.4	-292.3	-292.4	-292.6	-292.2
		0.6	545.5	0.972	91.4	91.0	92.3	90.9	89.7	92.3	539.5	738.3	738.4	738.3	738.4	738.4	738.3	-291.1	-291.2	-291.0	-291.2	-291.3	-291.0

632 **Table 4** Relative mass loss contributions (λ_i) of SCB constituents at different heating rate (β)

Heterogeneous kinetics model	β (K min^{-1})	PSE 1	PSE 2	PSE 3	OF (s^{-2})	fit (%)
A2	10	0.067	0.265	0.668	1.6×10^{-6}	85.8
	20	0.200	0.791	0.009	4.7×10^{-6}	86.9
	30	0.201	0.797	0.002	9.4×10^{-6}	87.1
	40	0.158	0.627	0.214	5.6×10^{-5}	74.7
	Average (±SD)	0.157 (±0.045)	0.620 (±0.177)	0.223 (±0.222)		
R2	10	0.126	0.590	0.284	1.5×10^{-6}	89.3
	20	0.157	0.603	0.240	5.2×10^{-6}	89.3
	30	0.127	0.590	0.283	9.9×10^{-6}	89.6
	40	0.127	0.591	0.283	1.5×10^{-5}	89.7
	Average (±SD)	0.134 (±0.012)	0.594 (±0.005)	0.272 (±0.016)		
R3	10	0.481	0.258	0.261	1.4×10^{-6}	89.8
	20	0.442	0.315	0.243	2.2×10^{-6}	93.0
	30	0.436	0.326	0.238	3.4×10^{-6}	93.9
	40	0.232	0.389	0.379	5.3×10^{-6}	93.9
	Average (±SD)	0.398 (±0.083)	0.322 (±0.035)	0.280 (±0.050)		
D2	10	0.508	0.305	0.187	7.1×10^{-8}	97.7
	20	0.441	0.320	0.239	1.2×10^{-6}	94.8
	30	0.690	0.201	0.110	6.0×10^{-6}	91.9
	40	0.184	0.287	0.529	9.1×10^{-6}	92.0
	Average (±SD)	0.456 (±0.143)	0.278 (±0.039)	0.266 (±0.131)		
D3	10	0.501	0.333	0.165	7.5×10^{-8}	97.6
	20	0.448	0.325	0.227	1.6×10^{-6}	94.0
	30	0.259	0.719	0.022	4.6×10^{-6}	92.9
	40	0.282	0.591	0.127	7.6×10^{-6}	92.7
	Average (±SD)	0.373 (±0.102)	0.492 (±0.163)	0.135 (±0.061)		
F1	10	0.514	0.374	0.112	4.5×10^{-7}	94.1
	20	0.473	0.339	0.188	1.9×10^{-6}	93.6
	30	0.481	0.354	0.166	4.3×10^{-6}	93.2
	40	0.476	0.373	0.151	8.0×10^{-6}	92.5
	Average (±SD)	0.486 (±0.014)	0.360 (±0.014)	0.154 (±0.023)		

633

Figure 1 Reaction scheme describing thermal degradation of major constituents from biomass

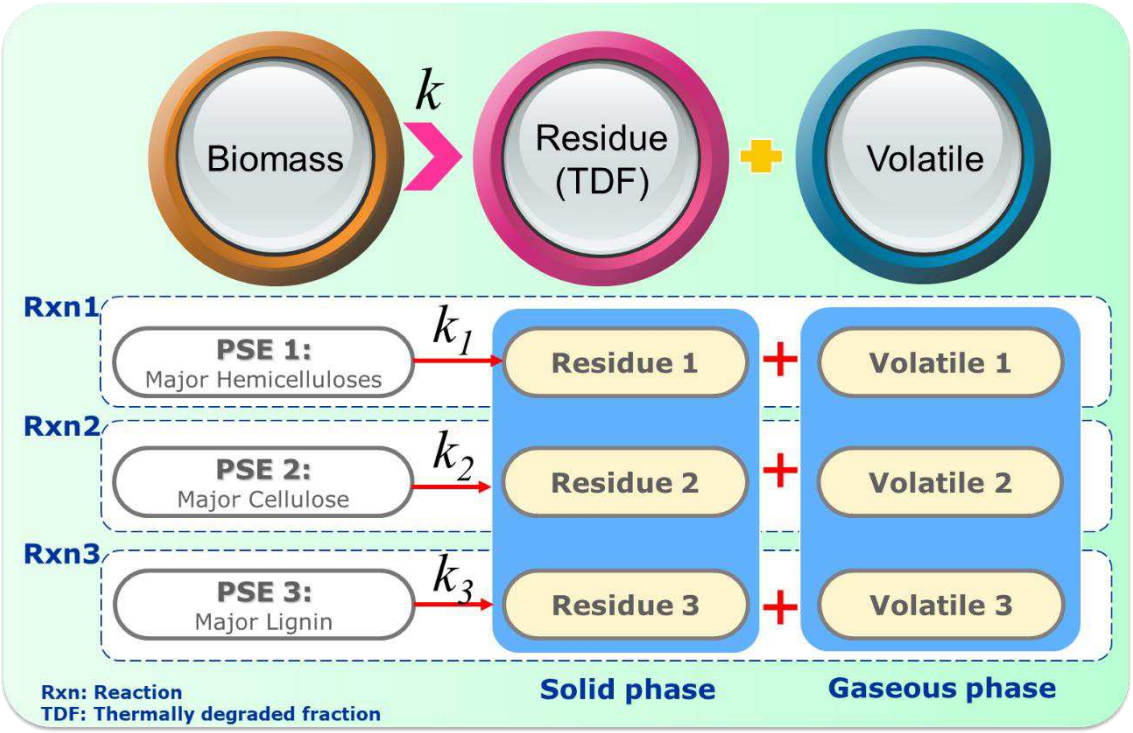

Figure 2 The deconvolution of three unresolved peaks (Dp) from the DTG curves of SCB samples at four heating rates under an inert atmosphere (N_2): (a) 10 K·min^{-1}, (b) 20 K·min^{-1}, (c) 30 K·min^{-1}, and (d) 40 K·min^{-1}

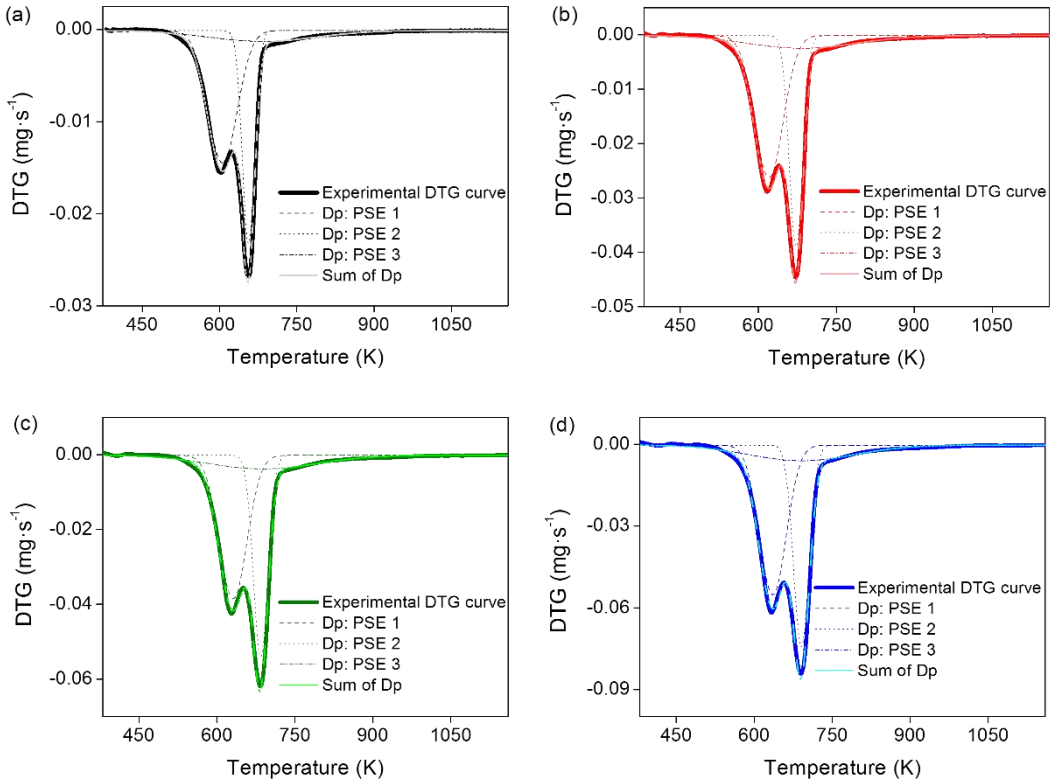

Figure 3 TG curves (dot lines), DTG curves (continuous lines), and conversion (dash lines) of the high polymers from SCB recorded at four heating rates: 10 K·min^{-1} (····,▬, ---), 20 K·min^{-1} (····,▬, ---), 30 K·min^{-1} (····,▬, ---) and 40 K·min^{-1} (····,▬, ---) under an inert atmosphere (N_2) for (a) PSE 1: hemicelluloses + extractives and lignin, (b) PSE 2: cellulose + extractives and lignin, and (c) PSE 3: lignin + extractives and residual holocellulose (hemicelluloses + cellulose)

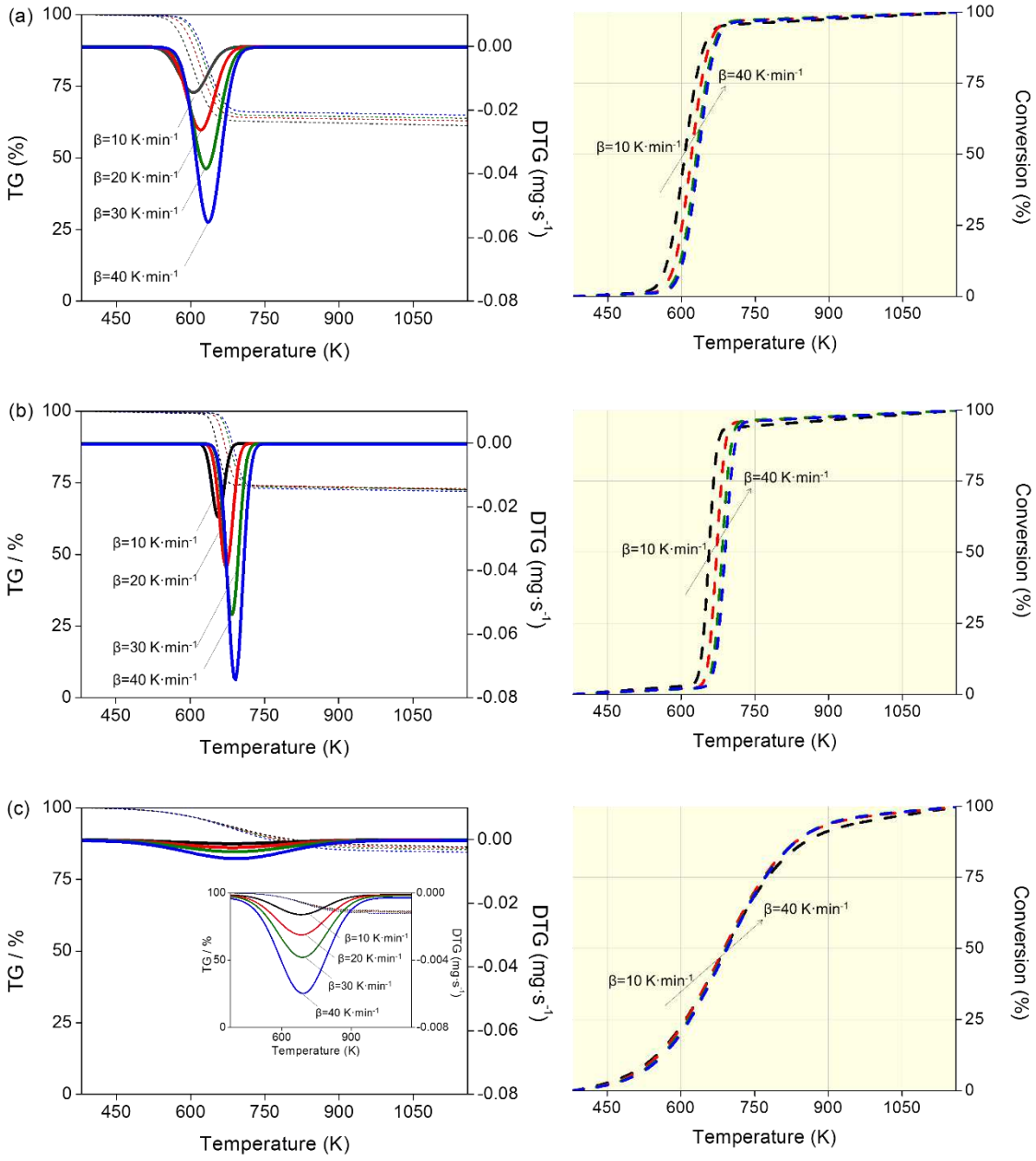

Figure 4 Kissinger plot of the values for $ln\left(\frac{\beta}{T_m^2}\right)$ as a function of ${T_m}^{-1}$. ▲ PSE 1: hemicelluloses+ extractives and lignin; ■ PSE 2: cellulose+ extractives and lignin; ● PSE 3: lignin+ extractives and residual holocellulose (hemicelluloses + cellulose); ---- linear fit

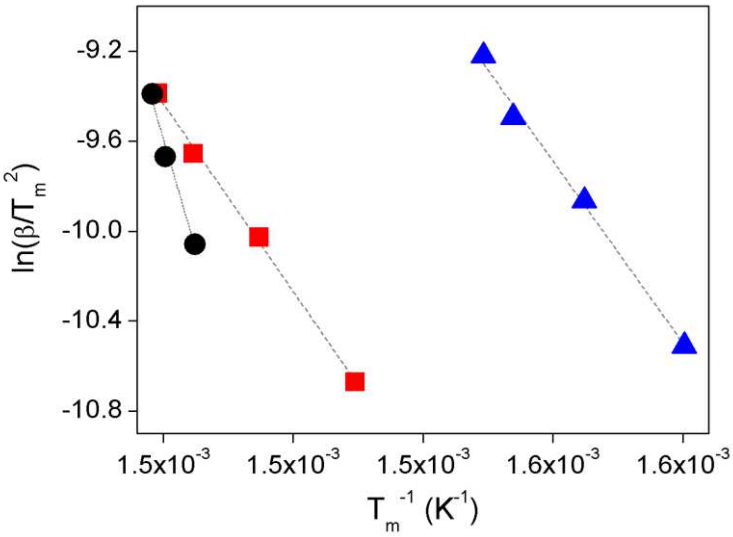

Figure 5 (a - c) Flynn–Wall–Ozawa (FWO) plots and (d - f) Kissinger-Akahira-Sunose (KAS) plots for the thermal degradation reactions and conversion degrees of α = 0.05; 0.1; 0.2; 0.3; 0.4; 0.5; 0.6; 0.7; 0.8; and 0.9; for: (a and d) PSE 1: Hemicelluloses + extractives and lignin, (b and e) PSE 2: Cellulose + extractives and lignin, and (c and f) PSE 3: Lignin + extractives and residual holocellulose (hemicelluloses + cellulose)

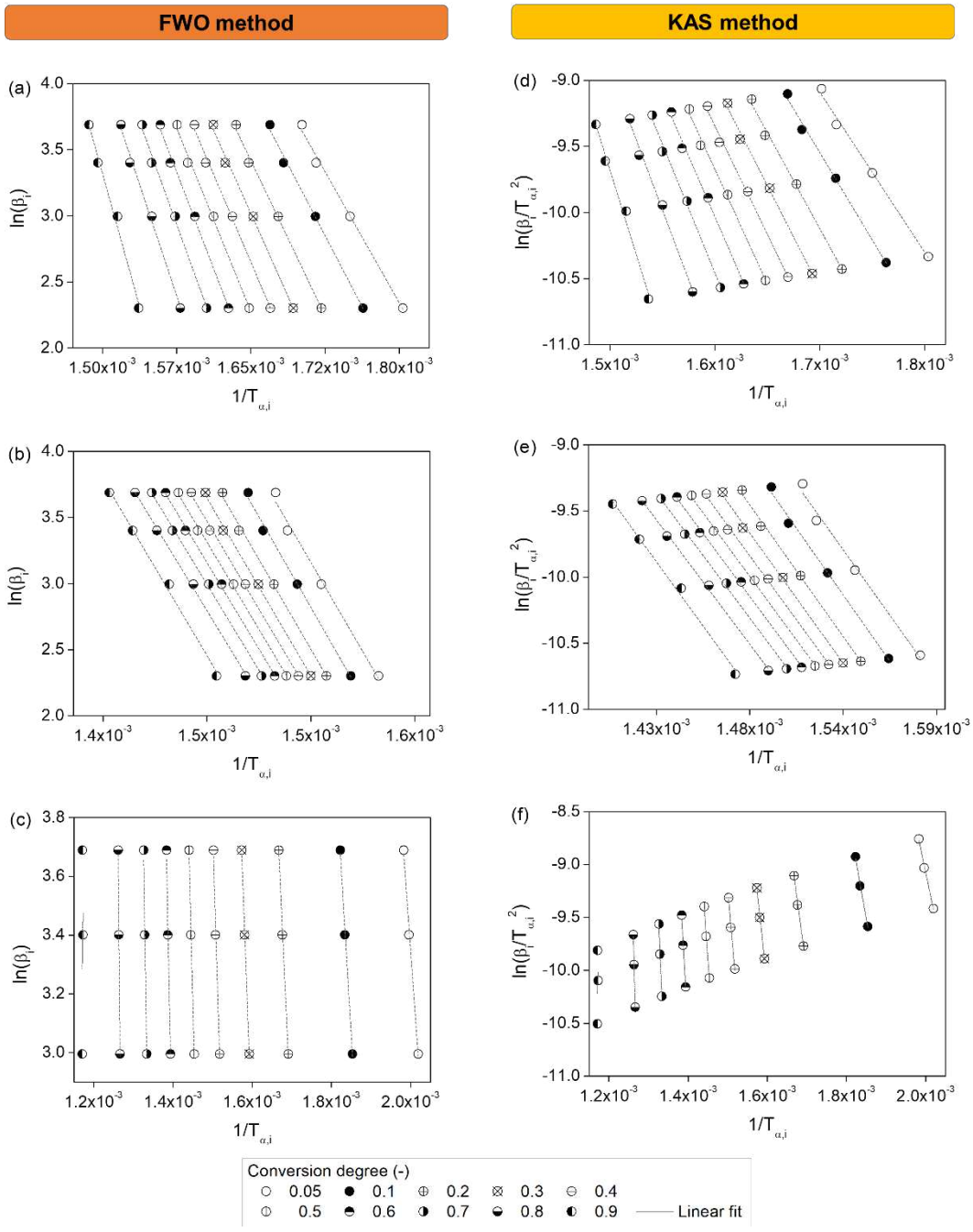

Figure 6 $\left.\frac{d\alpha}{dt}\right|_{cal}$ best-fit of thermal degradation of SCB compared with $\left.\frac{d\alpha}{dt}\right|_{exp}$ curves at 10 K·min^{-1}; 20 K·min^{-1}; 30 K·min^{-1}, and 40 K·min^{-1} using different f(α) models used in the heterogeneous kinetic: (a) A2 model; (b) R2 model; (c) R3 model; (d) D2 (model); (e) D3 model, and (f) F1 model

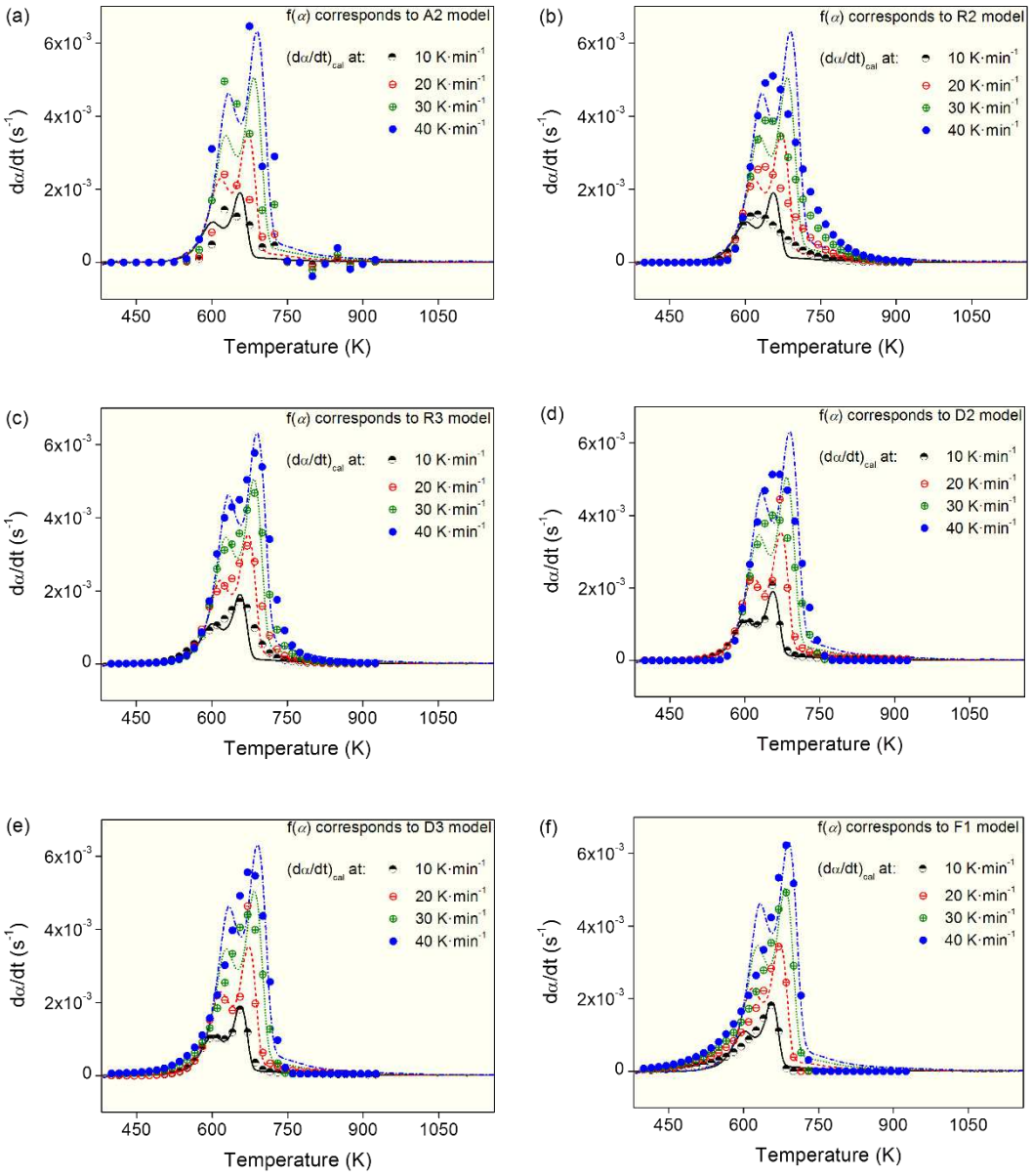

Figure 7 Thermal degradation fraction (TDF) corresponding to the parallel reactions scheme of (a) PSE 1: hemicelluloses + extractives and lignin, (b) PSE 2: cellulose + extractives and lignin, and (c) PSE 3: lignin+ extractives and residual holocellulose (hemicelluloses + cellulose)